

Optical and magnetic properties of doped ZnO: experimental and simulation

S. JANTRASEE^a, P. MOONTRAGOON^{b,c}, S. PINITSOONTORN^{b,c*}

^aMaterials Science and Nanotechnology Program, Faculty of Science, Khon Kaen University, Khon Kaen, Thailand

^bIntegrated Nanotechnology Research Center, Department of Physics, Faculty of Science, Khon Kaen University, Khon Kaen, Thailand

^cNanotec-KKU Center of Excellence on Advanced Nanomaterials for Energy Production and Storage, Khon Kaen University, Khon Kaen, Thailand

In this work, the effects of Al-, Ga- and Co-doping in the ZnO system on its optical and magnetic properties are presented. The work is divided into the experimental and simulation sections. Firstly, nanosized powders of $Zn_{1-x}M_xO$ ($M = Al, Ga$ and Co , $x = 0$ and 0.03) were synthesized using a hydrothermal method. The XRD results showed that the resulting powders were of a single phase with a hexagonal structure. The morphology of the samples revealed by SEM and TEM showed that they are different in shape and size. The optical properties of the samples, measured using a UV-VIS technique, exhibited strong absorption spectra below 400 nm in the UV region. This is equivalent to the band gap energy in the range of 3.21-3.97 eV. The type of dopants used have an influential effects on the absorption spectra. The magnetization curves at 300 K and 50 K were investigated using the VSM technique. The undoped ZnO and the Al- and Ga-doped ZnO exhibited only diamagnetic behavior whereas the Co-doped ZnO showed a combination of diamagnetism and ferromagnetism. Secondly, simulations were done using ABINIT software, which is based on density functional theory (DFT). The electronic structures (density of states) and the magnetic properties of the doped-ZnO were investigated using a PAW (projector-augmented plane wave) pseudopotential method within a local spin density approximation by the Hubbard model (LSDA + U). The optical and magnetic properties were extracted from the calculated results. Experimental and simulations results showed good agreement.

(Received April 11, 2016; accepted November 25, 2016)

Keywords: Doped- ZnO, Optical properties, Magnetic properties, Density functional theory

1. Introduction

Transparent semiconducting oxides have been intensively studied in recent years, which has led to a wide range of potential applications. One of the most promising transparent semiconducting oxides is a wurtzite-type Zinc Oxide (ZnO) as a candidate material for transparent electronics, sensors and solar cells [1]. ZnO doped with small amounts of transition metals, Co in particular, has been intensively investigated for use in diluted magnetic semiconductors (DMSs) [2]. DMSs based on III-V or II-VI semiconductors show ferromagnetism only at very low temperatures, but the oxide-based DMSs exhibited ferromagnetism at higher temperatures and even well above room temperature. The oxide-based DMSs are also optically transparent enabling them to be promising candidates for use in magneto-opto-electronic applications [3]. Starting from the initial work of Ohno et al. on Mn-doped GaAs, a ferromagnetic semiconductor with a $T_c \sim 110$ K [4], there have been continuous efforts to obtain such systems with high T_c . It is preferable for these materials to have a T_c close to room temperature [5, 6]. These investigations helped to develop a better understanding of the origin of ferromagnetism in this system. A wide variety experimental results fuel the debate on the origin of ferromagnetism in these systems, where a T_c above room tem-

perature was observed based on such diluted magnetic oxides. In experimental studies, the presence of long range ferromagnetic ordering was observed, and especially that the magnetic moment. In these studies, T_c depended on the details of sample preparation. Among the available metal dopants, Al- and Ga-doped ZnO have attracted much attention due to their electrical conductivity and optical properties. Al-doped ZnO has several advantages in terms of conductivity and thermal/chemical stability, while Ga-doped ZnO has superb properties for conductivity and durability in humid environments [7]. In recent years, many studies have used first principles calculations to investigate the effects of doping on various ZnO properties, such as crystal structure, electronic characteristics, and optical properties [8, 9]. Theoretical calculations can provide considerable insight into the microscopic characteristics of these materials, which can guide the future design of materials.

In this study, the optical and magnetic properties of nanosized powders of Al-, Ga- and Co-doped ZnO were investigated and compared with the results of first principles calculations. The synthesized powders were characterized using XRD, SEM, and TEM techniques. Optical absorption measured by UV-VIS spectroscopy was done to demonstrate the presence of the optical bandgap of the materials. The magnetic properties of $Zn_{1-x}M_xO$ ($M = Al,$

Ga and Co) powders with different particle sizes were investigated.

2. Experimental details

2.1. Synthesis details

In this work, $Zn_{1-x}M_xO$ ($M = Al, Ga$ and $Co; x = 0$ and 0.03) powders were prepared using a hydrothermal method. Zinc acetate dehydrate ($Zn(CH_3COO)_2 \cdot 2H_2O$ (AR Grade, Sigma-Aldrich)), aluminium nitrate nonahydrate ($Al(NO_3)_3 \cdot 9H_2O$ (AR Grade, Sigma-Aldrich)), gallium (III) nitrate hydrate ($Ga(NO_3)_3 \cdot xH_2O$ (AR Grade, Sigma-Aldrich)), and cobalt(II) acetate tetrahydrate ($Co(CH_3COO)_2 \cdot 4H_2O$ (AR Grade, Sigma-Aldrich)) were used as the starting raw materials. Firstly, we mixed aqueous solutions of zinc, aluminium, gallium and cobalt compounds in de-ionized water to form solutions in the ratio of $Zn_{1-x}M_xO$ ($x = 0$, and 0.03). Secondly, 1 mol of NaOH was added to the solution to cause precipitation. Thirdly, the precursor was synthesized using a hydrothermal method at $180^\circ C$ and 4 hours. After that, the precipitates were washed with copious quantities of de-ionized water. Then the precipitates at each M concentration were dried at $80^\circ C$ for 6 h. Finally, the $Zn_{1-x}M_xO$ nanocrystals were kept in a humidity-controlled cabinet at room temperature before characterization.

2.2. Characterizations

The phase composition and morphologies of $Zn_{1-x}M_xO$ ($M = Al, Ga$ and Co) nanoparticles were characterized using X-ray diffraction (XRD, PW3040 Philips, Eindhoven, Netherlands), scanning electron microscopy (SEM, LEO 1450VP, UK) and transmission electron microscopy (TEM, FEI Tecnai G2, Eindhoven, Netherlands). The optical properties of $Zn_{1-x}M_xO$ ($M = Al, Ga$ and Co) powders were measured using UV-Visible spectroscopy (UV-VIS). The magnetic properties of the $Zn_{1-x}M_xO$ ($M = Al, Ga$ and Co) powders were examined at low temperature (50 K) and room temperature (300 K) using a Vibrating Sample Magnetometer (VersaLab, Quantum Design, USA).

2.3. Computational details

Electronic and magnetic properties for $Zn_{1-x}M_xO$ ($M = Al, Ga$ and Co) were calculated via the first principles method based on a local density approximation (LDA+U) scheme with coulomb interaction (U_{eff} of Zn and Co were 9.0 and 6.88 eV respectively), using the ABINIT code [10]. The calculations were performed using self-consistent pseudo-potential projected augmented plane wave with LSDA+U formalism and the parametrization of Perdew and Wang [11] to explore the possibility of ferromagnetism as observed in recent experiments [12]. The $Zn_{1-x}M_xO$ ($M = Al, Ga$ and Co) with $x = 0.0000$ and 0.0625 were modeled using a $2 \times 2 \times 2$ supercell in the hexagonal wurtzite structure (space group P63mc). The

lattice parameters of the supercell were experimentally obtained from the results of the X-ray diffraction patterns ($a=b= 6.504 \text{ \AA}$ and $c = 10.424 \text{ \AA}$) without structural optimization. The supercell contained 32 atoms, which was eight times as large as the size of a primitive wurtzite unit cell in the base plane direction, as shown in Fig. 1. The orbitals of Al ($3s^23p^1$), Ga ($4s^23d^{10}4p^1$), Co ($3d^74s^2$), Zn ($3d^{10}4s^2$), and O ($2s^22p^4$) were treated as valence electrons. A $9 \times 9 \times 5$ Monkhorst-Pack k -point mesh was used for the zinc oxide supercell calculation. A projected augmented plane wave (PAW) with a cutoff energy of 16 Hartree was used to assure convergent results. The initial magnetic moment was set to zero for all atoms except for Co atoms, for which the initial moment was set to 3 Bohr magneton.

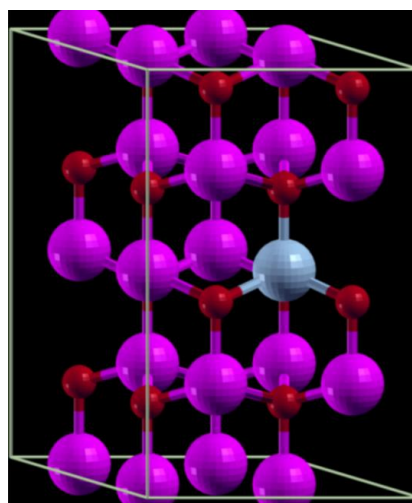


Fig. 1. The crystal structures of $Zn_{1-x}M_xO$ ($M = Al, Ga$ and Co), where the pink, red and light blue spheres represent Zn atoms, O atoms and the doped atoms, respectively.

3. Results and discussion

The synthesized powders were characterized for crystal phase identification using powder X-ray diffraction (XRD). The XRD patterns of the ZnO and doped ZnO powders (Fig. 2) showed the same peak patterns, which can be indexed as the ZnO wurtzite structure (JCPDS, 36-1451). This indicated that the wurtzite structure was not affected by Al or Co substitution. However, for the Ga-doped samples, the Ga_2O_3 impurities (-: JCPDS, 20-0426) were observed as the small peaks marked with asterisks. From the XRD patterns, the lattice parameters of the undoped and doped ZnO were determined and are shown in Table 1. The average crystallite sizes (D) for all the samples were calculated from the line broadening of all the observed XRD peaks using the Scherrer formula: $D = K_\alpha / \beta \cos \theta$, where λ is the wavelength of the X-ray radiation, K_α is a constant taken as 0.89, θ is the diffraction angle, and β is the full-width at half-maximum (FWHM) [13]. The average crystallite sizes of the ZnO, Al-, Ga- and Co-doped ZnO powders are also

shown in Table 1. The lattice parameters of all samples were not different significantly due to the relatively similar ionic radii of the cations and small concentration of the dopant. However, the intensity of the diffraction peaks decrease greatly with doping (Fig. 2), indicating a reduction in crystallinity due to lattice distortion.

Table 1. The lattice parameters and particle sizes of ZnO, Al-, Ga- and Co-doped ZnO

Material	Lattice parameters		Unit Cell Volume (\AA^3)	Crystallite size D (nm)
	a (\AA)	c (\AA)		
ZnO	3.252	5.212	47.73	62±10
Al-doped ZnO	3.253	5.203	47.68	53±9
Ga-doped ZnO	3.257	5.205	47.82	58±11
Co-doped ZnO	3.255	5.208	47.79	49±7

The morphology of the ZnO, Al-, Ga- and Co-doped ZnO powders are revealed in the SEM shown in Fig. 3. The powders doped with various materials were inhomogeneously agglomerated with particle sizes of ~300 nm. These figures show large spherical aggregates of smaller individual nanoparticles of various sizes. From Fig. 3a and b, it can be seen that the formation of nanoparticles was

self-aggregated in a close-packed periodic array of hexagonal-like shaped particles. The undoped ZnO and Al-doped ZnO show grains of sizes in the range of 0.8–1 μm with inter-granular spacing. Fig. 3(c, d) reveals the presence of randomly distributed spherical nanoparticles of Ga- and Co-doped ZnO with sizes ranging from 2–6 μm .

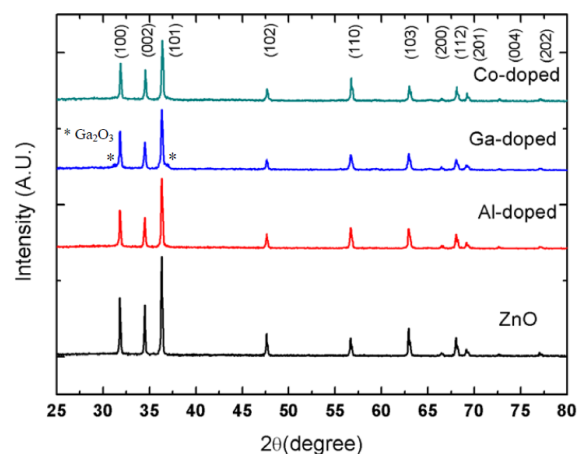


Fig. 2. XRD patterns of the pure and doped ZnO.

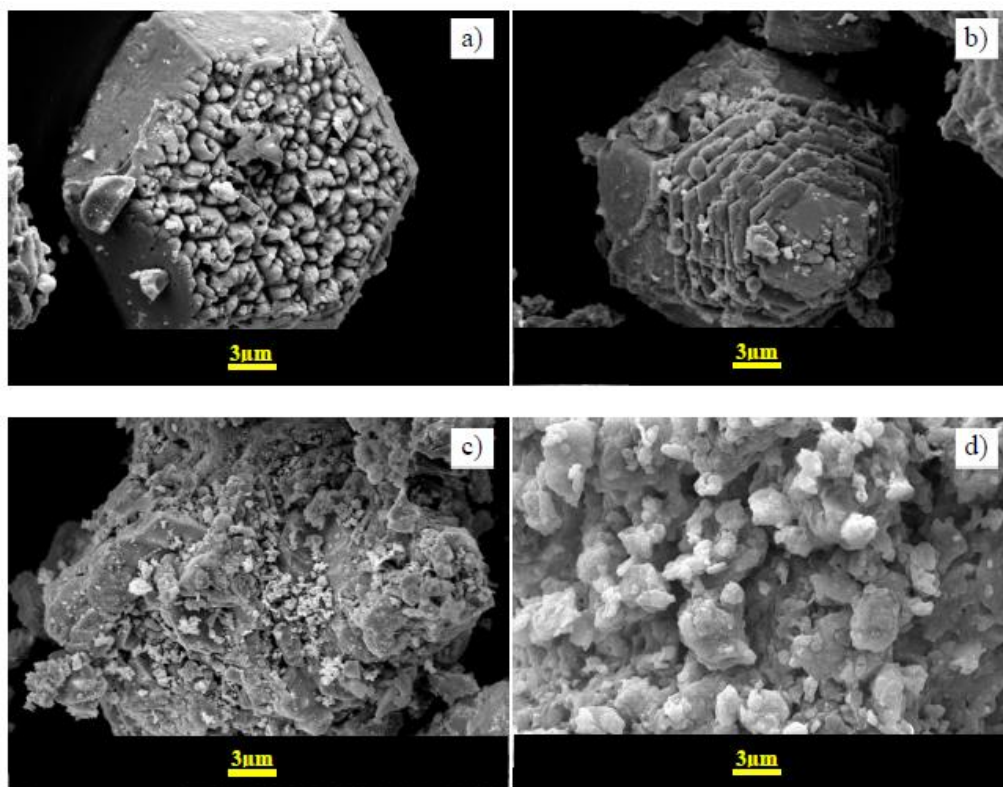


Fig. 3. SEM images of a) ZnO, b) Al-doped ZnO, c) Ga-doped ZnO, and d) Co-doped ZnO powders.

TEM images of ZnO, Al-, Ga- and Co-doped ZnO powders are shown in Fig. 4. These micrographs show that

the particle sizes increased when doping with other elements. The particle size of the pure ZnO sample ranged

from 10–45 nm, while the particle sizes of the Al-doped ZnO samples were larger (70–100 nm). The sizes of the Ga-doped ZnO and the Co-doped ZnO were range of 55–

105 nm and 250–300 nm, respectively. The TEM micrographs showed that doped ZnO nanocrystals had self-aggregated during the synthesis process.

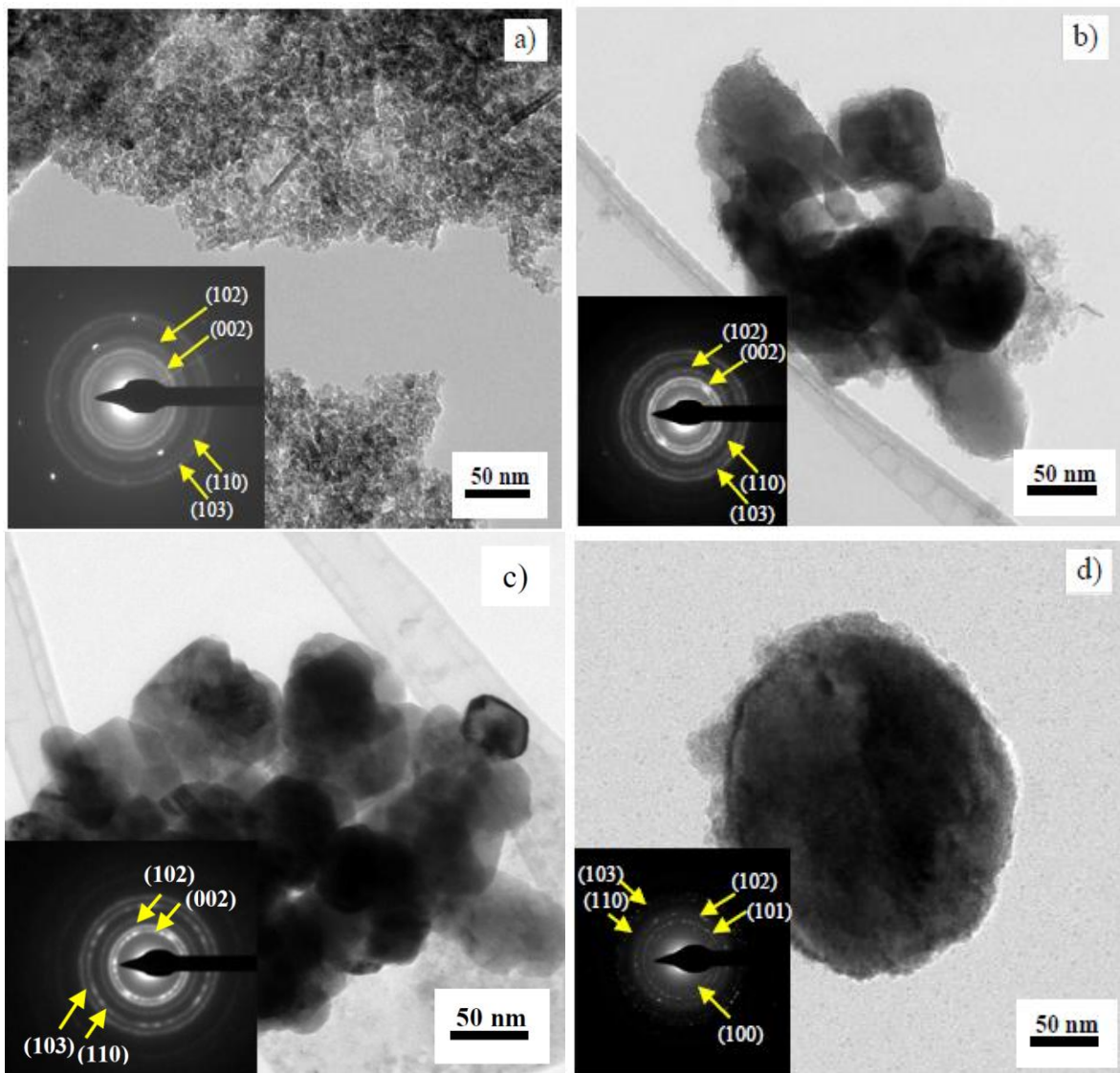


Fig. 4. TEM images of a) ZnO, b) Al-doped ZnO, c) Ga-doped ZnO, and d) Co-doped ZnO powders.

The optical properties of doped ZnO were compared with undoped ZnO to investigate the effect of doping on the band gap. UV–VIS absorption spectra of the doped ZnO powders in Fig. 5 show similar characteristics to the typical pure ZnO phase. The absorption edge of the Al-, and Ga-doped samples ($\lambda = 380$ nm) was also close to that of the undoped sample (376 nm) [14]. The Tauc method was implemented for calculating the optical band gap of the samples using the following equation [15]:

$$(\alpha h\nu)^n = A(h\nu - E_g) \quad (1)$$

where α , $h\nu$, A and E_g are absorption coefficient, photon energy, relation constant and optical band gap, respectively. For semiconductors with a direct band gap, n

$= 2$, and for an indirect band gap, $n = 0.5$. In this study, the optical band gap was calculated with the direct band gap. Plotting $(\alpha h\nu)^2$ versus photon energy ($h\nu$) and extrapolation of the linear part to the photon energy axis resulted in the band gap value. The optical band gap of ZnO, Al-, Ga-, and Co-dopants were 3.69, 3.19, 3.21 and 3.97 eV, respectively. A redshift of the band gap with incorporation of Al, Ga into ZnO was observed. The decrease in the energy gap appeared to originate from the active transitions involving 3d levels in Al^{3+} or Ga^{3+} ions and strong sp - d exchange interaction between the itinerant sp carriers (band electrons) and the localized d electrons of the dopant [16]. Alternatively, the widening of the optical bandgap was due to the Burstein-Moss effect [17]. The Burstein-Moss effect explains that the excitation of an electron from the valence band to conduction band in a doped semicon-

ductor needs more energy due to the accumulation of the excessive electrons in the conduction band. Accordingly, the optical band gap was increased by Co doping.

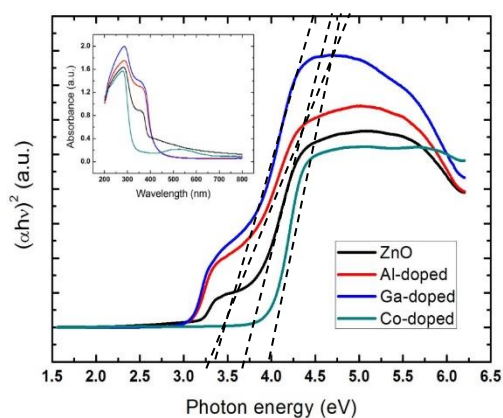


Fig. 5. Plot of $(ahv)^2$ versus photon energy (hv) , and the extrapolation of the linear parts of ZnO and Al-, Ga-, Co-doped ZnO. (Inset) UV-visible absorption spectra of ZnO and Al-, Ga-, Co-doped ZnO.

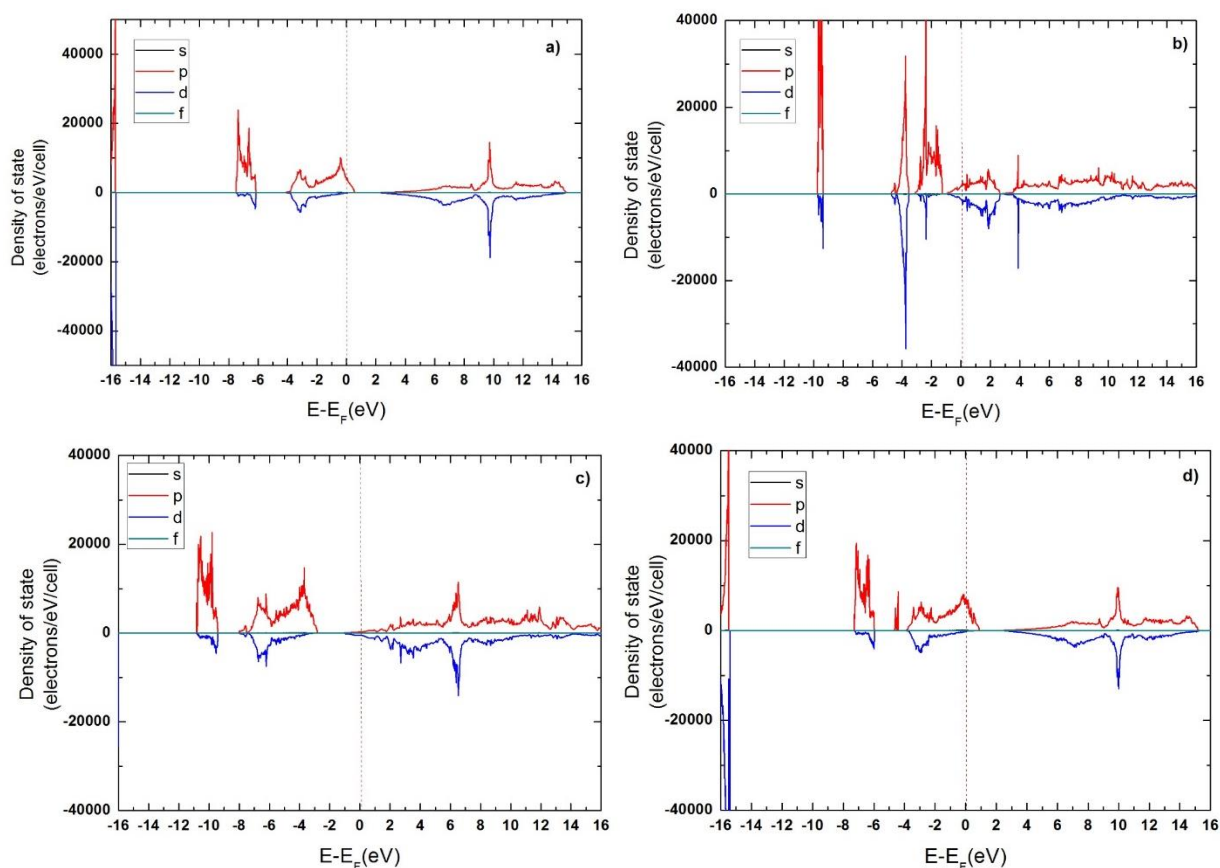


Fig. 6. The density of state of a) ZnO, b) Al-doped ZnO, c) Ga-doped ZnO, and d) Co-doped ZnO.

The magnetic properties of the undoped and doped ZnO powders were examined at room temperature using a vibrating sample magnetometer (VSM). The magnetization versus magnetic field ($M-H$) curves measured at 300 K are shown in Fig. 7. The linear relationship between the magnetization and applied magnetic field can be observed

The density of states (DOS) of pure ZnO and doped ZnO are shown in Fig. 6. For the undoped ZnO (Fig. 6a), the orbitals in the lower valence band (around -4 eV) were primarily Zn 3d, whereas the orbitals in the higher valence band (~ 0.5 eV) were mainly O 2p. The dominant contributors to the conduction band were the Zn 4s and Zn 4p orbitals, with a few O 2s and O 2p orbitals. Following the replacement of a Zn atom with an Al or Ga or Co atom (Fig. 6 b-d), the electrons occupying the lowest level of the conduction band caused the Fermi level to move upward into the conduction band, which produced typical n-type metallic characteristics. The calculated energy band gap of the undoped ZnO was about 1.75 eV, which is in good agreement with the other calculations. However, this value is still underestimated when compared to the experimental value (a direct band gap of 3.69 eV). The energy band gaps of Al-, Ga- and Co-doped ZnO were 1.22, 1.41 and 1.57 eV, respectively (Fig. 6 b-d). In Fig. 6d, for Co-doped ZnO, it is primarily the Co 3d states that contribute to the sharp peak between -5 and -3 eV. The Co 4s and Co 3d states contribute to the conduction band.

in ZnO, Al- and Ga-doped ZnO. Undoped ZnO, Al- and Ga-doped ZnO exhibited purely diamagnetic behavior, whereas the Co-doped ZnO showed a combination of diamagnetism and ferromagnetism. It can be clearly seen that in the field range of ± 2 kOe, the Co-doped ZnO sample exhibited an S-shape curve characteristic of ferromag-

netism [18]. The M-H curves at low temperature (50 K) and room temperature (300 K) of Co-doped ZnO, after subtraction of the diamagnetic signal, are shown in Fig. 8. It can be seen that the ferromagnetic part can be saturated in a field of 2 kOe. The values of M_s of Co-doped ZnO at 50 K and 300 K were 1.49×10^{-2} emu/g and 1.12×10^{-2} emu/g, respectively. These values are equivalent to the magnetic moment of 4.31×10^{-4} and 3.24×10^{-4} Bohr magneton (μ_B) per unit cell at 50 K and 300 K, respectively.

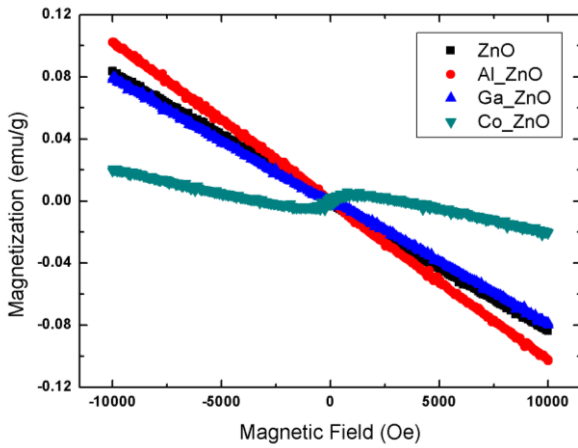


Fig. 7. Magnetization of ZnO, Al-, Ga-, and Co-doped ZnO with an applied magnetic field at 300 K.

The magnetic moments of the undoped and doped ZnO supercells were calculated from the ABINIT code. According to the LSDA+U calculation, the magnetic moments per unit cell of pure ZnO, $\text{Al}_{0.0625}\text{Zn}_{0.9375}\text{O}$, $\text{Ga}_{0.0625}\text{Zn}_{0.9375}\text{O}$ and $\text{Co}_{0.0625}\text{Zn}_{0.9375}\text{O}$ were $0 \mu_B$, $4.01 \times 10^{-12} \mu_B$, $4.45 \times 10^{-12} \mu_B$ and $0.374 \mu_B$, respectively. The computer simulations showed that only the Co-doped sample exhibited ferromagnetic behavior, and only Co atoms possess a magnetic moment, whereas for other atoms (Zn and O), the magnetic moments were nearly zero. The magnetic properties of the Co-doped zinc oxide from theoretical calculation can be described by superexchange theory in which the exchange interaction happens only on the Co and O sides, not on Zn and O sides [12]. The origin of magnetic moments of $\text{Co}_{0.0625}\text{Zn}_{0.9375}\text{O}$ can be visualized from the partial DOS of Co atoms as shown in Fig. 9. The difference between spin up and spin down electrons in the partial DOS resulted in the magnetic moments.

It should be noted that the results of our experimental and theoretical calculations are significantly different. This may be due to the effect of temperature since the calculated values are for the magnetic moment were at 0 K. Another explanation is the magnetic clusters of Co oxides in the experiment showed antiferromagnetic behavior and did not contribute to total magnetization. However, the measured values from our experiments are very close to other experimental reports [19, 20]. Similarly, the values from

our calculations are of the same order of magnitude as other simulations [21, 22].

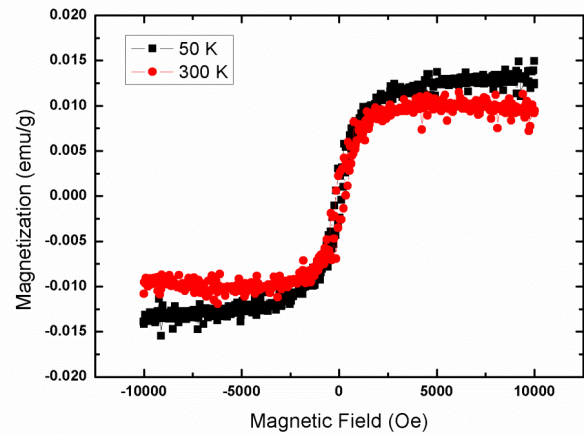


Fig. 8. Magnetization of Co-doped ZnO at 50 K and 300 K.

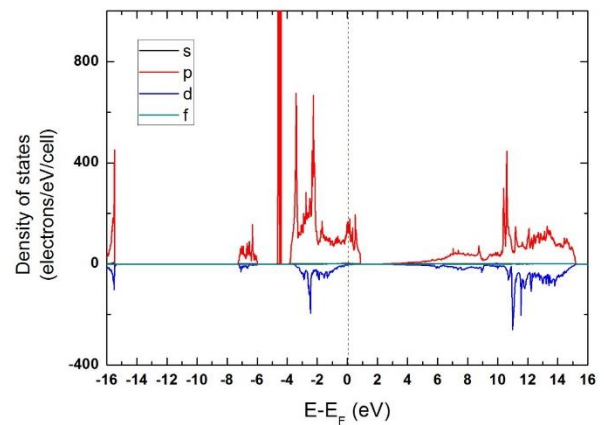


Fig. 9. Partial density of states (PDOS) for Co atoms in $\text{Co}_{0.0625}\text{Zn}_{0.9375}\text{O}$.

4. Conclusion

In summary, the optical and magnetic properties of $\text{Zn}_{1-x}\text{M}_x\text{O}$ ($M = \text{Al}, \text{Ga}$ and Co) nanoparticles with wurtzite structure, synthesized via a hydrothermal method, were investigated. The DFT + U_{eff} calculations were performed to evaluate the electronic structure and optical properties of the ZnO and the Al-, Ga-, and Co-doped ZnO system. The calculated results of the optical band gap and the magnetization of ZnO are consistent with experimental results. Correlation between the crystallite size and the measured properties were not found since the crystallite sizes of all samples were of the same order. Comparing with the optical band gap of ZnO, the Co-doped ZnO shows an increased band gap, while the band gap of the Al- and Ga-doped samples are decreased. The magnetic properties of the undoped ZnO, Al- and Ga-doped ZnO exhibited purely diamagnetic behavior, whereas the Co-

doped ZnO showed a combination of diamagnetism and ferromagnetism.

Acknowledgments

The authors would like to express their appreciation for the financial support from the National Research University Project of Thailand, Office of the Higher Education Commission, through the Advanced Functional Materials Cluster of Khon Kaen University and the Nanotechnology Center (NANOTEC), NSTDA, Ministry of Science and Technology, Thailand, through its program of Center of Excellence Network.

References

- [1] C. Jagadish, S. Pearton, *Zinc Oxide Bulk : Thin Films and Nanostructures Processing, Properties and Application*, Elsevier, Oxford, 2006.
- [2] J. K. Furdyna, *J. App. Phys.* **64**, R29 (1988).
- [3] I. Žutić, J. Fabian, S. Sarma, *Rev. Mod. Phys.* **76**, 323 (2004).
- [4] H. Ohno, *Science* **281**, 951 (1998).
- [5] K. Sato, Y. H. Katayama, *Physica E* **10**, 251 (2001).
- [6] U. Kenji, T. Hitoshi, K. Tomoji, *Appl. Phys. Lett.* **79**, 953 (2001).
- [7] T. Minami, *Semicond. Sci. Technol.* **20**, S35 (2005).
- [8] A. Janotti, C. G. Van De Walle, *Rep. Progr. Phys.* **72**, 126501 (2009).
- [9] Z. Zang, A. Nakamura, J. Temmyo, *Mater. Lett.* **92**, 188 (2013).
- [10] X. Gonze, B. Amadon, P. M. Anglade, J. M. Beuken, F. Bottin, P. Boulanger, F. Bruneval, D. Caliste, R. Caracas, M. Cote, T. Deutsch, L. Genovese, F. Ghosez, M. Giantomassi, S. Goedecker, D. R. Hamann, P. Hermet, F. Jollet, G. Jomard, S. Leroux, M. Mancini, S. Mazevet, M. J. T. Oliveira, G. Onida, Y. Pouillon, T. Rangel, G. M. Rignanese, D. Sangalli, R. Shaltaf, M. Torrent, M. J. Verstraete, G. Zerah, J.W. Zwanziger, *Comput. Phys. Commun.* **180**, 2582 (2009).
- [11] J. P. Perdew, Y. Wang, *Phys. Rev. B.* **45**, 13244 (1992).
- [12] P. Moontragoon, S. Pinitsoontorn, P. Thongbai, *Microelectron. Eng.* **108**, 158 (2013).
- [13] B. Cullity, S. R. Stock, *Elements of X-ray Diffraction*, Prentice-Hall, New Jersey, 2001.
- [14] M. Bouloudenine, N. Viart, S. Colis, A. Dinia, *Chem. Phys. Lett.* **397**, 73 (2004).
- [15] V. Srikant, D. Clarke, *J. Appl. Phys.* **83**, 5447 (1998).
- [16] N. Bahadur, A. K. Srivastava, S. Kumar, M. Deepa, B. Nag, *Thin Solid Films* **518**, 5257 (2010).
- [17] Z. Gibbs, A. Lalonde, G. Snyder, *New J. Phys.* **15**, 1 (2013).
- [18] S. Maensiri, J. Sreesongmuang, C. Thomas, J. Klinkaewnarong, *J. Magn. Magn. Mater.* **301**, 422 (2006).
- [19] V. Gandhi, R. Ganesan, H. H. A. Syedahamed, M. Thaiyan, *J. Phys. Chem. C*, **118**, 9715 (2014).
- [20] M. Shatnawi, A. M. Alsmadi, I. Bsoul, B. Salameh, G. A. Alna'washi, F. Al-Dweri, F. El Akkad, *J. Alloys Compd.* **655**, 244 (2016).
- [21] S. Hu, S. Yan, M. Zhao, L. Mei, *Phys. Rev. B* **73**, 245205 (2006).
- [22] J. Zhang, K. L. Yao, Z. L. Liu, G. Y. Gao, *Physica B* **405**, 1447 (2010).

*Corresponding authors: psupree@kku.ac.th